Systems/Circuits

Connectivity and Neuronal Synchrony during Seizures

Xin Ren,[1] Anastasia Brodovskaya,[2] John L. Hudson,[3*] and Jaideep Kapur[4]

[1]School of Engineering and Applied Science, University of Virginia, Charlottesville, Virginia 22904, [2]Neuroscience Graduate Program, University of Virginia, Charlottesville, Virginia 22908, [3]Department of Chemical Engineering, University of Virginia, Charlottesville, Virginia 22904, and [4]Department of Neurology & UVA Brain Institute, University of Virginia, Charlottesville, Virginia 22908

There is uncertainty regarding when and which groups of neurons fire synchronously during seizures. While several studies found heterogeneous firing during seizures, others suggested synchronous neuronal firing in the seizure core. We tested whether neuronal activity during seizures is orderly in the direction of the excitatory neuronal connections in the circuit. There are strong excitatory connections laterally within the septotemporally organized lamella and inhibitory trans-lamellar connections in the hippocampus, which allow testing of the connectivity hypothesis. We further tested whether epileptogenesis enhances synchrony and antiseizure drug administration disrupts it. We recorded local field potentials from CA1 pyramidal neurons using a small microelectrode array and kindled rats by a rapid, recurrent hippocampal stimulation protocol. We compared cross-correlation, theta phase synchronization, entropy, and event synchronization. These analyses revealed that the firing pattern was correlated along the lamellar, but not the septotemporal, axis during evoked seizures. During kindling, neuronal synchrony increased along the lamellar axis, while synchrony along the septotemporal axis remained relatively low. Additionally, the theta phase distribution demonstrated that CA1 pyramidal cell firing became preferential for theta oscillation negative peak as kindling progressed in the lamellar direction but not in the trans-lamellar direction. Last, event synchronization demonstrated that neuronal firings along the lamellar axis were more synchronized than those along the septotemporal axis. There was a marked decrease in synchronization and phase preference after treatment with phenytoin and levetiracetam. The synchrony structure of CA1 pyramidal neurons during seizures and epileptogenesis depends on anatomic connectivity and plasticity.

Key words: **hippocampus; lamellar; levetiracetam; phenytoin; septotemporal; synchrony**

Significance Statement

We could improve the efficacy of brain stimulation to treat seizures by understanding the structure of synchrony. Electrical stimulation may disrupt seizures by desynchronizing neurons, but there is an uncertainty on which groups of neurons fire synchronously or chaotically during seizures. Here, we demonstrate that neurons linked by excitatory connections fire synchronously during seizures, and this synchrony is modulated by epileptogenesis and antiseizure drugs. Closed-loop brain stimulation carefully targeted to disrupt synchrony may improve the treatment of seizures.

Introduction

Seizures were once defined as "a transient occurrence of signs and/or symptoms because of abnormal excessive or synchronous neuronal activity in the brain" (Fisher et al., 2014). High amplitude spike-wave discharges that occur during seizures represent the activity of a large group of neurons (Schevon and Trevelyan, 2014). Intracellular recordings from neurons during epileptiform bursts demonstrate a characteristic large depolarizing shift in membrane potential, called paroxysmal depolarizing shift. Synaptic potentials in individual neurons are synchronized and amplified by reduced GABAergic inhibition or enhanced excitatory transmission, generating a paroxysmal depolarizing shift in individual neurons and epileptiform spikes on EEG (Johnston and Brown, 1984; Miles et al., 1984; De Curtis and Avanzini, 2001).

A more complex picture of neuronal synchrony during seizures has emerged from multielectrode recordings from neurons in the cortex of patients undergoing evaluation for epilepsy surgery. Initial studies using microelectrode arrays designed to discern individual neuronal firing found a very heterogeneous activity without hypersynchronization among hundreds of neurons activated during a seizure (Truccolo et al., 2011). Other

Received Mar. 30, 2021; revised July 21, 2021; accepted July 25, 2021.

Author contributions: X.R. and J.K. designed research; X.R. performed research; X.R. analyzed data; X.R. wrote the first draft of the paper; X.R., A.B., and J.K. wrote the paper; A.B., J.L.H., and J.K. edited the paper; J.L.H. contributed unpublished reagents/analytic tools.

*Deceased.

This work was supported by National Institutes of Health Grants RO1 NS040337, RO1 NS119012, AND UO1 NS58204 PR093963, Department of Defense, and Congressionally Directed Medical Research Program. We thank John Williamson for assistance with the experiments.

The authors declare no competing financial interests.

Correspondence should be addressed to Jaideep Kapur at jk8t@virginia.edu.

https://doi.org/10.1523/JNEUROSCI.0669-21.2021

studies describe a seizure propagating in a core, with a penumbra shaped by an inhibitory surround (Schevon et al., 2012). There is synchronous neuronal firing in the ictal core, where paroxysmal depolarizing shifts can be recorded, but not in the penumbra region (Merricks et al., 2015).

In theoretical and *in vitro* models, excitatory synaptic connectivity between principal neurons allows neuronal synchrony (Wong et al., 1986; Johnson et al., 2015). Extensive positive feedback excitation mediated by recurrent axon collaterals connecting the CA3 pyramidal neurons, which project directly to CA1 neurons, combined with intrinsic bursting properties of these neurons, suggests that they can rapidly synchronize and propagate bursts, resulting in seizures (Traub and Wong, 1982; Traub et al., 1989; McCormick and Contreras, 2001). The hippocampus is proposed to have a simple, functional organization of excitatory connections along lamellae extending from the entorhinal cortex to granule cells, CA3, CA1 pyramidal neurons, and the subiculum (Andersen et al., 1971). Detailed anatomic analysis of the hippocampus suggests a more complex structure with information processing along the transverse and long axis. However, the lamellar organization has remained a useful functional concept, and lateral inhibition activated by granule cells keeps lamella functionally separate (Sloviter et al., 2006; Sloviter and Lømo, 2012). This lamellar connectivity would suggest that synchronous neuronal activity would propagate along the lamellar axis, whereas they would not do so along the trans-lamellar axis. However, most studies testing these hypotheses were conducted in brain slices; therefore, hippocampal seizure propagation patterns in freely moving animals are still undeveloped. While many studies have yielded deep insights into synchronization (D. Lee, 2002; X. Li et al., 2007; Lenck-Santini and Holmes, 2008), there is still no consensus on which quantitative measurement of synchrony is the best way of defining relationships within and between brain regions.

We tested whether CA1 neuronal networks' lamellar connectivity plays a role in determining their synchronization during seizures. Neuronal connectivity is enhanced during epileptogenesis by various mechanisms, thus facilitating the synchronization of connected neuronal networks. Furthermore, we expected that antiseizure medications would interfere with neuronal synchrony. We recorded local field potentials using small microelectrode arrays in the CA1 region in animals that underwent kindling epileptogenesis *in vivo*. Electrodes were arrayed either along the septotemporal or lamellar axis. We applied four measures of synchrony.

Materials and Methods

Animals. All protocols were approved by the University of Virginia Animal Care and Use Committee. Adult male Sprague Dawley rats (250-300 g) were housed 2 per cage on a light/dark cycle in a temperature-controlled room with access to food and water.

Kindling. A rapid kindling protocol was used for freely moving rats. According to the protocol, stimuli trains (10 s, 50 Hz, 1 ms biphasic pulses) were delivered at 30 min intervals 10-12 times per day (Lothman et al., 1985). We measured after-discharge duration (ADD) from the end of the stimulus to the end of the evoked seizure. We ranked seizure severity according to the Racine scale (see Fig. 1*E*) (Racine, 1972). The animals were fully kindled when they had a minimum of three Stage 5 seizures in succession. After completing the recording, the animals were killed via CO_2 asphyxiation. Electrode positions were confirmed via histologic examination, as described below. The brains were removed and stored in a 1% potassium ferricyanide and 4% PFA in a 0.1 M PB at 4°C overnight. Potassium ferricyanide reacts with residual iron from the electrodes to form Prussian blue, aiding in electrode placement confirmation. Brains were then frozen and sectioned perpendicular to the septotemporal axis (on a sliding microtome) at 40 μm. The electrode locations appeared as azure spots on the slices. We confirmed the location of the recording sites for all animals used in this study.

Local field potentials. We constructed bipolar electrodes from two equal lengths of 500 μm stainless-steel coated wires (A-M System) (see Fig. 1*B*). The wires were twisted and cut at an angle to prevent short-circuiting between the tips. We fabricated the microelectrode array from 8 strands of 50 μm nichrome-coated wires (10 μm coating, A-M System), which were lined up with a tool and then glued together (see Fig. 1*A*). A spacing wire separated adjacent electrodes (50 μm nichrome-coated wire) about the pyramidal cell soma diameter. The recording sites were 100 μm apart from center to center. After several hours, the tips were cut transversely on the same surface level with sharp scissors. Before implantation, the electrode tips were examined under a microscope to ensure no superglue was present at the exposed surface. The impedance of each electrode was typically 25-40 kΩ.

The rats were anesthetized with isoflurane, placed in a stereotaxic frame, and maintained on a heating pad (37.5°C). A bipolar electrode, implanted in the hippocampal CA3 (AP −3 mm; ML, 3.5 mm; DV, 2.5-3.0 mm below the dura), was used for delivering stimulus pulse trains. We implanted a microelectrode array in the contralateral hippocampal CA1 region (AP, 3.0 mm; ML, 2.0 mm; DV, 2-2.5 mm below the dura) along the transverse or longitudinal hippocampal axis for recording field potentials. We optimized the microelectrode array position in the CA1 pyramidal cell layer by recording responses to Schaffer collateral stimulation. A coated stainless-steel wire (1 mm, A-M System) was placed in the skull to serve as the reference electrode. Our interpretation assumes that each signal channel of the microelectrode array records from a unique set of neurons with minimal crosstalk because the spike waveform changes between channels during the evoked seizures showed that the electrodes could record from different groups of neurons in the densely packed CA1 pyramidal cell layer (see Fig. 1*B*). Microelectrode design was based on the theory that extracellular field potentials are local current sinks, or sources, generated by the collective action potentials of many neurons (Brette and Destexhe, 2012). A negative wave corresponds to a current sink, caused by positive charges entering cells through postsynaptic glutamate receptors, whereas a positive wave is generated by the current that leaves the cell (at the cell body) (Richardson et al., 1987; Andersen et al., 2009). Figure 1*B* shows field potentials recorded at various positions along the length of the soma and dendritic tree. The waveform of the spike varied as a function of distance from the cell body. The population of spikes (red star) was negative when recording from the cell body layer. This observation supports the assumption that the waveform of a single spike can be quite different depending on the recording site. We did not record a single unit because the goal of these experiments was to detect interactions between high-frequency firing in a small, local region in the hippocampal CA1 layer. Therefore, knowing that each electrode represents a small group of neurons was sufficient for our analysis.

The microelectrode array signals were buffered with an operational amplifier attached to a lightweight headset (gain = 1). The operational amplifiers were connected to 4-channel amplifiers (A-M Systems, model 1700) via flexible cables through a rotating commutator. The analog output port of the amplifier was connected to an analog input channel of the DAQ system. The DAQ system consisted of two computers: a real-time controller and a LabVIEW-based host computer. The controller used a high-speed Field Programmable Gate Array processor to acquire data at a 25 kHz sampling rate, yielding a resolution of 40 μs. The LabVIEW-based host computer was used for the postprocessing and visualization of the experimental data. The recording was continuous before, during, and after the electrically kindled seizures. All microelectrode array channels were recorded from 1 Hz to 10 kHz and later passed through a high-pass filter of 300 Hz for offline high-frequency firing analysis.

Spike rate. We detected spike peaks and troughs using a MATLAB peak finder on the filtered data. We coded the peak finder to find the local maximums and minimums and calculated during the evoked

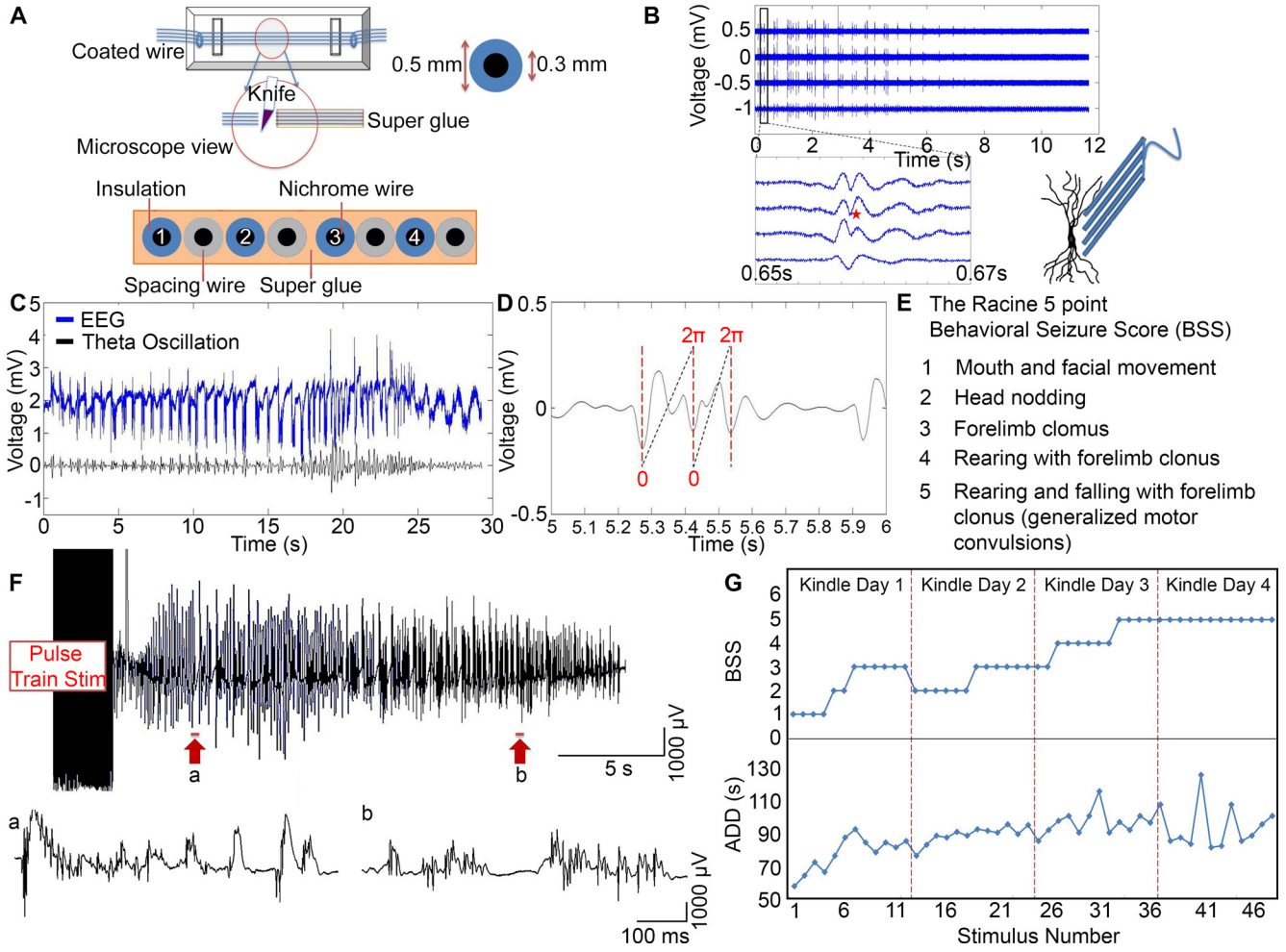

Figure 1. Kindling progression in awake rats. ***A***, Schematic of the microelectrode construction and dimensions of the outer and inner diameters of the wire. The tips were cut transversely with a sharp knife and examined under a microscope to make sure no Superglue was attached on the cross section surface. Each of the 4 microelectrodes was separated by an additional 50 μm spacing wire. ***B***, The waveform of a spike varied as a function of distance from the cell body. Schematic figure represents microelectrode array placement along the somatodendritic axis. Four channels of bandpass-filtered data (300-4000 Hz): An electrically evoked seizure was immediately recorded after 10 s of stimulation. Enlarged view, Waveform of a single spike (red star). ***C***, Top, EEG signal. Bottom, Theta oscillation. ***D***, The waveform is the theta oscillation. Red dotted lines indicate the negative peaks of the theta oscillation. The theta cycle is defined as the time between two negative peaks. Each time point is assigned with a theta phase value from 0 to 2 via linear interpolation. ***E***, The Racine 5 point BSS. ***F***, Top, A representative example of an electrically evoked seizure that was recorded in an awake rat immediately after 10 s of stimulation. The EEG was filtered >1 Hz. Bottom, ***a***, ***b***, Expanded views of two segments of the EEG data, taken from the sections indicated by the arrows beneath the top trace. ***G***, A representative example of BSS and ADD as they increased in severity during 4 d kindling for 1 animal.

seizures. The sample sizes between groups were comparable. The code is available on request.

Measures of synchrony. We used cross-correlation, phase synchronization, and event synchronization (ES) to measure synchrony. The signal from the microelectrode array was filtered between 300 and 4000 Hz before synchronization analysis. We only analyzed low-noise and artifact-free EEG recordings.

Cross-correlation estimates the degree of correlation between two different time-series, where the cross-correlation coeffcient r is as follows:

$$r = \frac{\sum_i^N (x_i - m_x)(y_i - m_y)}{\sqrt{\sum_i^N (x_i - m_x)^2}\sqrt{\sum_i^N (y_i - m_y)^2}},$$

where m_x and m_y are the means of series, and N is the number of samples in them. Correlation coeffcients were calculated across all pairwise combinations across the duration of a seizure (see Fig. 3*E*).

Theta oscillations. The EEG signal was first passed through a fourth-order Butterworth filter with theta band cutoffs (between 4 and 10 Hz) to extract the theta oscillation (see Fig. 1*C*). The Butterworth filter can reduce the ripples in the output signals, which smooth out the signal. We only treated the troughs below certain values (for example, −0.1) at the beginning or end of the cycle; each rat could have a different baseline. We used the baseline (nonseizure) to calculate the mean and SD of the signal. Later, we used mean + 3 SD for the spike detection. Theta phase is linearly increased from 0 to 2 from one negative peak to the next. For this definition of synchronization, which does not calculate the instantaneous phase of the oscillation, the change in the phase is of interest, and amplitude is largely irrelevant because we have already considered the baseline shift in the code. In the case of neuronal firings, the peaks of action potentials were assigned with theta phase values that were determined by the firing time within that phase window (see Fig. 1*D*). The propagation pattern in the hippocampus CA1 region was evaluated by calculating the phase differences between firing groups. The phase difference can be any value from 0 to 2.

For the theta phase difference distributions, we first found all the firing spikes (action potentials, see below) in all four channels. Then, we defined the theta cycle (see above). Next, we calculated the spike phase in the theta cycle. Finally, we calculated the difference between the spike phases for each pair of the channels and show the distribution in histogram plots.

Shannon entropy. Shannon entropy measures the order state of a sequence and quantifies the degree of skew in the distribution. We used it to quantify the order of theta phase distributions, using the following:

$$\text{Shannon entropy}\,(S) = -\sum_i p_i ln(p_i), p_i > 0,$$

with $S_{max} = ln\, M$, where M is the number of bins, and π is the probability of the phase difference being in the i-th bin. For complete desynchronization, the value is zero.

ES. The definition of ES is less stringent, where synchronization only implies that defined events are occurring simultaneously, or near-simultaneously, in time (Quian Quiroga et al., 2002). We defined population bursts as discrete events in time and calculated synchronization from the near-simultaneous occurrence of population bursts within a small time window (the synchronization window was set to 30/25,000 Hz = 1.2 ms). We identified population bursts as bursts >3 SDs from the baseline (seizure-free EEG over 10 min). ES quantifies the number of times an event occurs in two-time series and does not require the notion of phase. Given recordings from two electrodes of the microelectrode array, time series x and y, the event times are defined as t_i^x and t_j^y. Population bursts that occur in both signals within a time interval are considered to be synchronized. The number of times an event appears in x shortly after it appears in y is defined as follows:

$$C^{\tau}(x|y) = \sum_i^{n_x} \sum_j^{n_y} J_{ij}^{\tau}$$

$$J_{ij}^{\tau} = \begin{cases} 1 if 0 < t_i^x - t_j^y < \tau \\ \frac{1}{2} if t_i^x = t_j^y \\ 0 otherwise \end{cases}$$

where n_x is the number of spikes in neuron x, and n_y is the number of bursts for the neuron y. The values of $C^{\tau}(x|y)$ and $C^{\tau}(y|x)$ are then combined symmetrically (Q) and anti-symmetrically (q):

$$Q_{\tau} = \frac{C^{\tau}(x|y) + C^{\tau}(y|x)}{\sqrt{n_y n_x}}$$

$$q_{\tau} = \frac{C^{\tau}(x|y) - C^{\tau}(y|x)}{\sqrt{n_y n_x}},$$

where Q is the strength of the ES. Q varies from 0 to 1, with 0 being non-synchronized events and 1 being completely synchronized events.

Antiepileptic drug (AED) treatments. We implanted a microelectrode array along the lamellar axis in CA1. We stimulated the animals until a minimum of three Stage 5 behavioral seizures had occurred to ensure fully kindled state. After the drug injection, the same stimulus was delivered 8 more times, once every 30 min for 4 h (when the recording ended) to the CA3 region of the hippocampus. We used measures of synchrony described above.

Statistics. The minimum level for determining significance was $p < 0.05$. Data are reported as mean ± SD unless noted otherwise. The statistical tests used were the Student's t test (MATLAB), ANOVA (MATLAB), and the Kruskal–Wallis test (MATLAB). *Post hoc* multicomparison tests were done using the Tukey method (MATLAB). The Kolmogorov–Smirnov test (MATLAB) was used to test whether the difference in spike rate during different epochs was significant.

Data availability. The data that support the findings and codes are available from the corresponding authors on request.

Results

Higher firing frequency during more intense seizures in the lamellar, but not septotemporal, recording configuration

We kindled animals using rapidly recurring hippocampal stimulation. The behavioral seizures became more intense, and ADDs were longer with repeated stimulation, with large variation in between, because after a long seizure, there is a postictal depression that shortens the next seizure (Fig. 1*G*) (Herberg and Rose, 1994; Pottkämper et al., 2020). The morphology of the firings changed throughout the seizure (Fig. 1*F*). Animals were kindled until they reached three successive Behavioral Seizure Score (BSS) 5 seizures; we excluded 3 of 23 rats that failed to kindle fully.

We recorded the neuronal activity during seizures in both the lamellar and septotemporal configurations (Fig. 2*A*,*B*). Different recording sites, which correspond to the microelectrode array's electrodes, varied in their response latencies to the stimulation. In the lamellar configuration, seizures showed a growing preference for high-frequency activities as the seizure progressed (Fig. 2*C*,*E*). We observed high-frequency oscillation events throughout the seizure. More high-frequency activities occurred during Stage 5 seizures than the less intense seizures (Fig. 2*E*). In contrast, in the septotemporal direction, during Stage 5 seizures, firing frequencies were similar to Stage 1 seizures (Fig. 2*D*,*F*). The high-frequency component (>300 Hz) increased as the seizure stage advanced (Fig. 2*G*,*H*).

We calculated the cross-correlation coeffcients across all pairwise combinations against time. In individual kindled seizures ($n = 90$), CA1 neuronal activities were less correlated at the beginning and toward the end of the kindled seizures. However, they were highly correlated in the middle of the seizure (Fig. 3*A*, *B*). During an electrically evoked seizure in the lamellar configuration, the correlation coeffcients initially increased (0.42-0.84), stayed steady (0.68-0.9) in the middle, and were disrupted (0.2) toward the end.

In the septotemporal configuration, the correlation coeffcients fluctuated randomly between −0.29 and 0.33 throughout the seizure (Fig. 3*C*,*D*). The negative correlation coefficients indicated that, when the voltage of one channel increased, the voltage of another channel decreased. Since these coeffcients were quite small compared with those of the lamellar configuration, it is not surprising that there was little to no correlation in the septotemporal direction.

We provide examples of the cross-correlation coefficients across all pairwise combinations with microelectrodes placed along the lamellar direction. During kindling in awake rats, the correlation between neuronal activities in different channels diminished with increasing stimuli (Fig. 3*E*). Neurons in awake rats were very active, resulting in complex discharges as kindling progressed (Fig. 3*F*). The complex discharges caused the morphology of the burst waveform to be highly variable, resulting in a less correlated state. Therefore, correlation is not a robust method to quantify synchronization. In contrast, phase analyses robustly demonstrated neuronal synchrony increased as kindling progressed (Fig. 3*G*). The relationship between neuronal firing and theta oscillation is crucial in understanding synchronization in the hippocampus. In awake rats, CA1 pyramidal cells fired preferentially around the negative peak of theta oscillation with an increasing number of stimuli (as will also be described below).

Theta phase synchronization shows neuronal synchrony increased in the lamellar direction as kindling progressed but not in the septotemporal direction

We recorded 150 evoked seizures from 6 animals with the microelectrode array placed along the lamellar axis, where theta phase analysis of these seizures robustly demonstrated neuronal synchrony increased as kindling progressed (Fig. 4*A*). During the

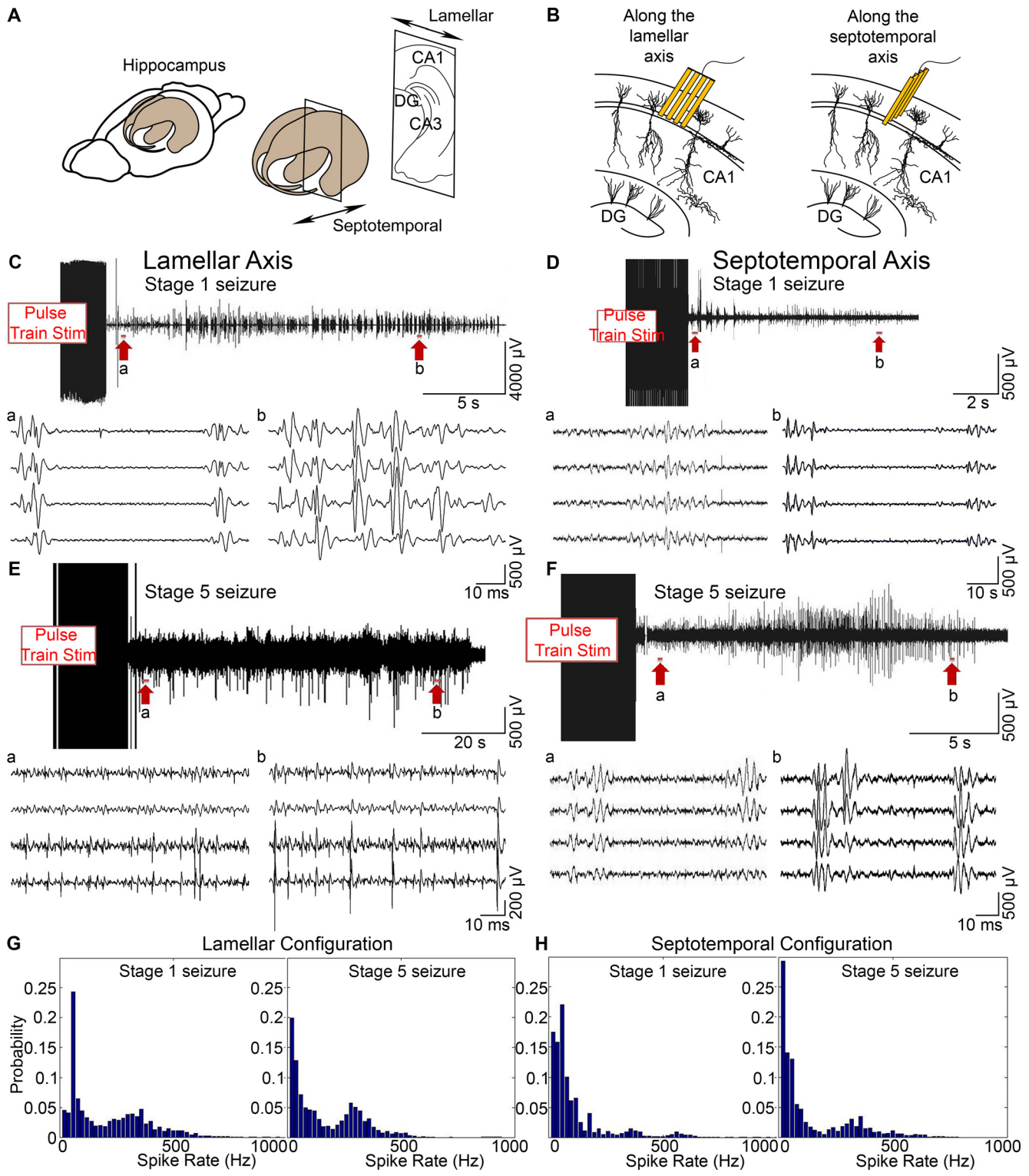

Figure 2. High-frequency firing and spike rate distributions along the lamellar and septotemporal axes. ***A***, The rat hippocampus is indicated in both the lamellar and septotemporal directions. ***B***, Schematic figures of the microelectrode array placement in the hippocampal CA1 cell layer. ***C***, ***E***, High-frequency firing along the lamellar axis. EEG was filtered between 300 and 4000 Hz to extract high-frequency firing data. High-frequency firing during a Stage 1 seizure (***C***) and a Stage 5 seizure (***E***). Top traces, One channel of the filtered seizure data. Bottom, ***a***, ***b***, Expanded views of the top traces indicated by the arrows. ***D***, ***F***, High-frequency firing along the septotemporal axis. High-frequency firing during a Stage 1 seizure (***D***) and a Stage 5 seizure (***F***). ***G***, ***H***, Spike rate distributions during kindling. Spike rates of Stage 1 and Stage 5 seizures in the lamellar configuration (***G***) and the septotemporal configuration (***H***).

early stages of kindling, the phase value was randomly spread evenly between 0 and 2 π in the lamellar configuration, indicating a random relationship between CA1 cell firing and theta rhythm (Fig. 4*C*). For Stage 5 seizures, the phase distribution showed a preferred value of ~1.8, close to the troughs of the theta oscillations, suggesting that local neuronal firings become more strongly influenced by the slow theta oscillations (Fig. 4*E*). Additionally, the marked transition from unaffected to strongly affected indicates that firings had become more organized during kindling.

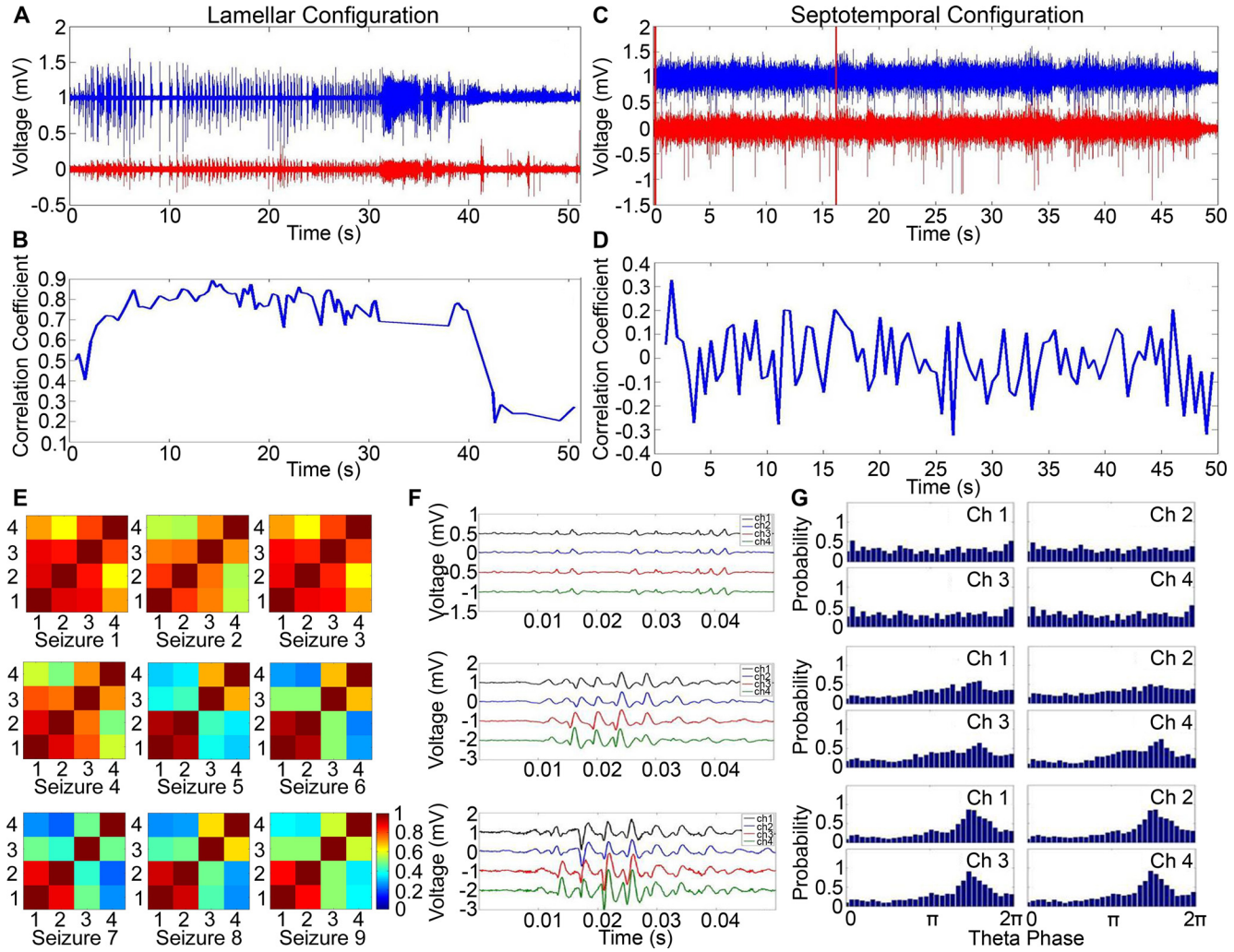

Figure 3. A representative example of the correlation profile between two channels of the microelectrode array recording during seizures in awake rats. EEG data from two channels of the microelectrode array are plotted next to each other and the correlation coefficient against time in the lamellar configuration (***A***,***B***) and septotemporal configuration (***C***,***D***). ***E***, The cross-correlation coeffcients across all pairwise combinations in awake rats in the lamellar direction. ***F***, Discharge morphology as kindling progressed. ***G***, Progression of theta oscillations with increasing number of stimulus.

We calculated the theta phase difference distributions between all pairs of the channels. For the early-stage seizures, all six distributions were negatively skewed (Fig. 4*F*). The median and mean were negative for all distributions, which indicate that the firing was recorded by one channel followed by the other channel. The microelectrode array was placed along the CA1 lamellar axis so that channel one was close to the hippocampal CA3 region (Fig. 4*B*). The neuronal firings recorded by the microelectrode array reveal propagation where Channel 1 led Channel 2, which followed Channel 3, which leads to Channel 4. This pattern indicates that the seizure originates in hippocampal CA3 because of direct CA3 stimulation and then propagates through the transverse extent of the monitored CA1 cell layer. Thus, the firings propagate from the proximal to distal electrode along the lamellar axis. However, we cannot exclude that the baseline activity within a circuit could be responsible for the ictal propagating activity.

The histograms of the theta phase difference distributions during both the early and final stages of kindling are shown in Figure 4*D* as a comparison. Both distributions are skewed to the negative side, suggesting that the propagation pattern is preserved throughout the kindling process. Theta phase difference is also an indicator of how synchronized the channels are because the distribution becomes progressively more skewed toward zero as the animal is kindled. This means that fully kindled animals (Fig. 4*D*) are much more likely to exhibit simultaneous firing across all channels at the zero components of the theta phase distributions, suggesting increased synchronized activity.

We next recorded seizures ($n = 145$) in 6 rats in the septotemporal direction, and the phase value was randomly spread as kindling progressed (Fig. 4*G*). We did not find exactly the same theta phase distributions in Figure 4*A*, *G* in the initial Stage 3 kindling because recordings in the lamellar and septotemporal directions were done in different rats, and the probabilities would slightly vary. There could be slight stereotaxic differences during surgery, rat size/sex variability, and natural rat to rat firing variability. However, the shown examples are not extremes, and we did not find the same increased theta phase synchrony in the septotemporal direction as we did in the lamellar in fully kindled Stage 5 animals. If the difference was because of the just recording location, we would not be able to see such a drastic difference in the theta phase distribution between initially and fully kindled animals. The theta phase distributions recorded from septotemporal electrodes were spread randomly between 0 and 2 π at both the early and fully kindled stage (Fig. 4*H*). The neuronal firings did not interact with the underlying theta oscillations,

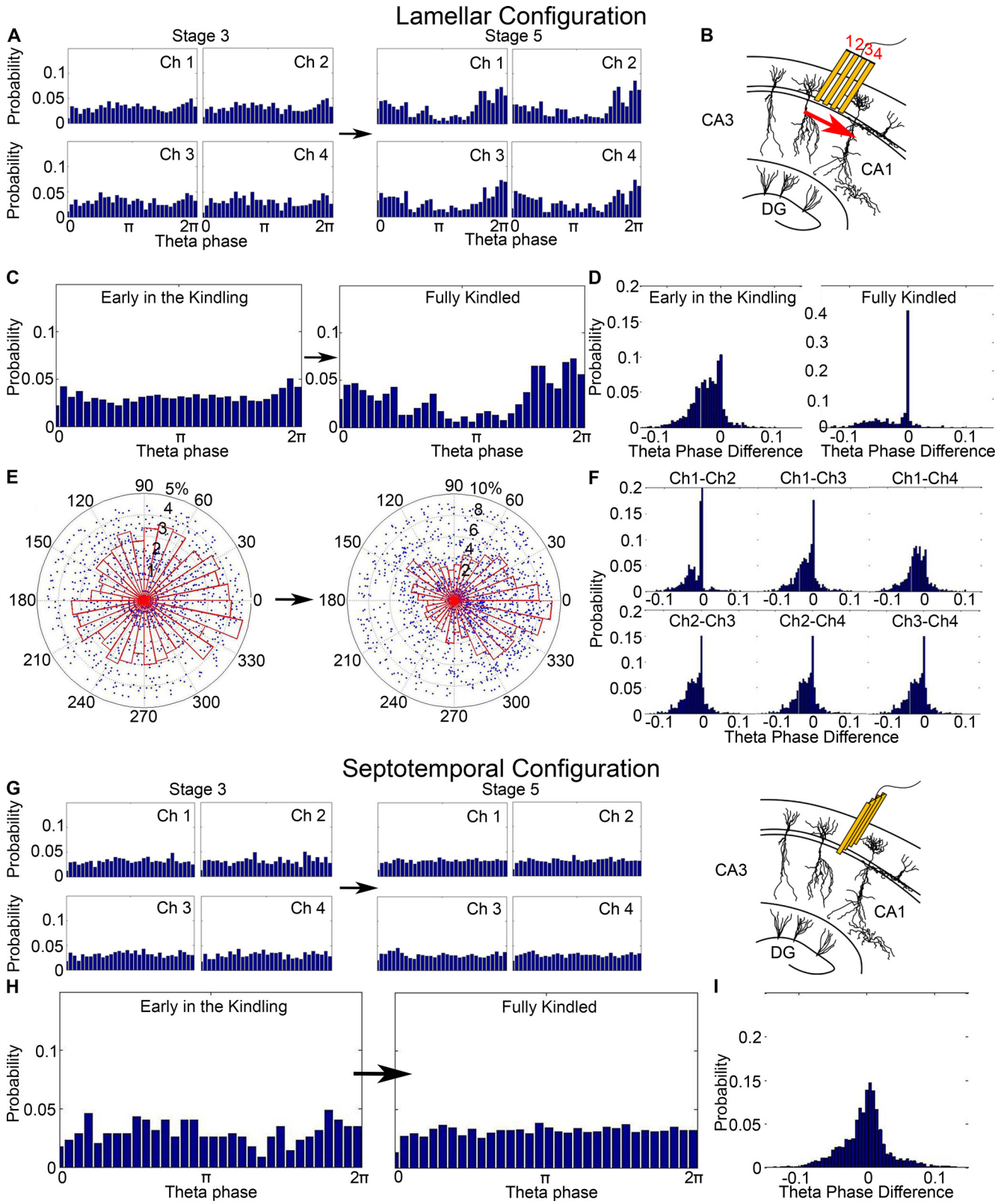

Figure 4. Theta phase distribution in the lamellar and septotemporal configurations. ***A***, Theta phase analysis demonstrates that neuronal synchrony increased in the lamellar microelectrode array configuration as kindling progressed. ***B***, Schematic plot of the firing propagation pattern in hippocampal CA1. Red arrow indicates the direction of propagation from Channel 1 to Channel 4 along the lamellar axis from proximal to distant direction. ***C***, Theta phase distribution in the lamellar configuration in the early and late stage of the kindling that showed a preferred firing phase for Stage 5 seizures. ***D***, Theta phase difference distributions in the early and fully kindled stage. Both distributions are negatively skewed, which means that the propagation pattern is sustained throughout the kindling process. ***E***, Circle plot of the data in ***C***, graphed from 0 to 2 pi. Histogram represents the probability. Dots represent the theta phase values and standardized population bursts for each firing. The radius is the standardized population burst. The further it is from the center, the higher the population burst. ***F***, In early-stage seizures, theta phase difference distributions among all pairs of the four channels are negatively skewed, which indicates that a propagation pattern between the channels of the microelectrode array progresses in a proximal to distal manner. ***G***, Theta phase distribution shows that, for the entire kindling, the phase value randomly spread between 0 and 2 pi. ***H***, Theta phase distributions in the

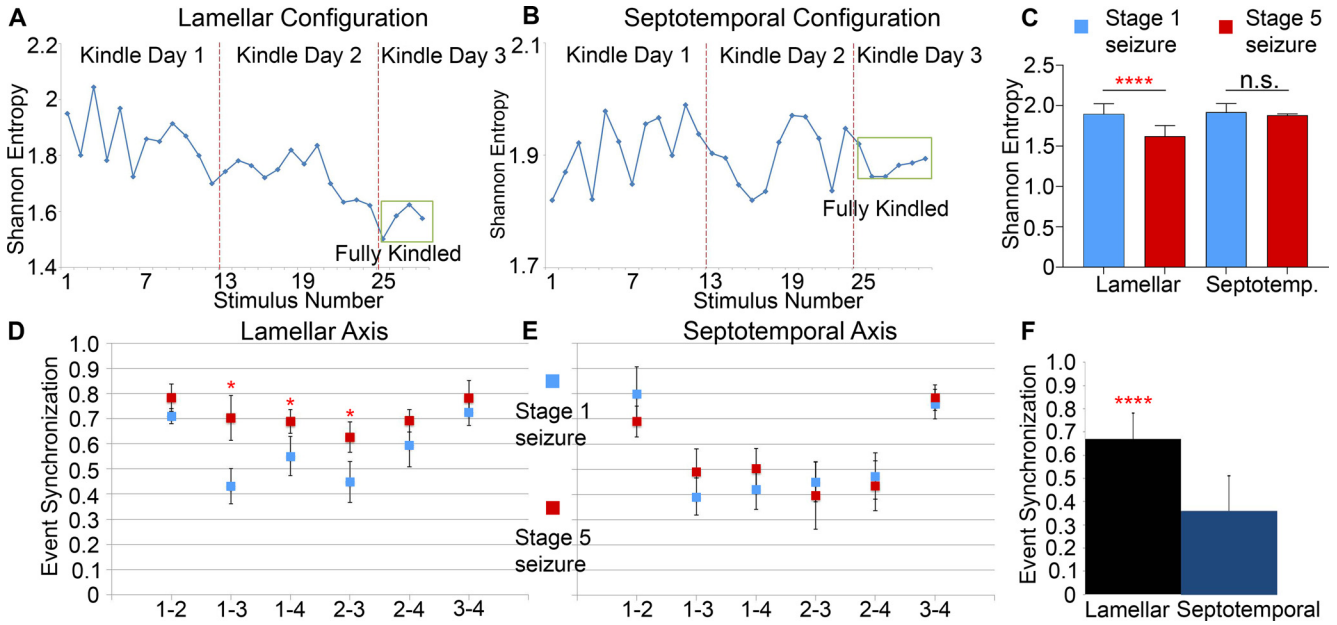

Figure 5. Shannon entropy and ES along the lamellar and septotemporal axes. ***A***, Shannon entropy attenuated as kindling progresses in the lamellar configuration. ***B***, Shannon entropy fluctuated as kindling progressed along the septotemporal axis but showed no significant changes between stages. ***C***, Grouped mean Shannon entropy between four channels for Stage 1 (blue) and Stage 5 (red) seizures in the lamellar and septotemporal configurations. As the BSS advanced from Stage 1 to Stage 5, the entropy level dropped for all four channels in the lamellar, but not septotemporal, configuration (paired *t* test). ***D***, ES increased as kindling progressed along the lamellar axis. Blue squares represent Stage 1 seizures. Red squares represent Stage 5 seizures. ***E***, ES showed no significant difference as kindling progressed along the septotemporal axis. ***F***, ES was significantly higher in the lamellar direction than the septotemporal direction. ****$p < 0.0001$.

nor was a preferred firing phase observed in the septotemporal direction (Fig. 4*I*).

Shannon entropy decreased in the lamellar configuration as kindling progressed but stayed the same in the septotemporal configuration

Shannon entropy was calculated to quantify the degree of order in the theta phase distributions. Shannon entropy decreased as kindling progressed in the lamellar configuration (Fig. 5*A*, $n = 150$ seizures, 6 rats, $p < 0.05$, ANOVA). As the BSS stage advanced from 1 to 5, the entropy level dropped for all four channels (Fig. 5*C*). The mean grouped Shannon entropy for all four channels in the lamellar direction was 1.90 ± 0.13 for Stage 1 seizures, and it decreased significantly to 1.62 ± 0.13 at the fully kindled stage ($p < 0.0001$, paired *t* test). A large decrease in entropy quantitatively demonstrates that neuronal synchrony increased in the small monitored area as kindling progressed. It shows that, during more severe seizures, the neurons are more synchronized.

In seizures ($n = 145$) with septotemporally placed microelectrode array in 6 rats, the average Shannon entropy did not show a linear increase or decrease, fluctuating between 1.82 and 2.00 (Fig. 5*B*). The mean grouped Shannon entropy for all four channels did not show any difference during Stage 1 (1.88 ± 0.017) or Stage 5 seizures (1.92 ± 0.11) (Fig. 5*C*, $p = 0.17$, paired *t* test), indicating that the synchrony level was homogeneous in the small recording area throughout kindling. The neuron groups recorded by each electrode were not distinguishable from each other. Compared with the lamellar configuration, the average Shannon entropy along the septotemporal axis remained relatively high throughout kindling, meaning that neurons did not become more synchronized as kindling progressed.

ES shows neuronal synchrony increased in the lamellar direction as kindling progressed but not along the septotemporal direction

We analyzed all of the recorded seizures and calculated the mean and SD of the ES strength. Neuronal firings along the lamellar axis were more synchronized (Fig. 5*F*, ES strength = 0.67 ± 0.19) compared with septotemporal axis (ES strength = 0.36 ± 0.18, $p < 0.001$, paired *t* test).

ES examined the synchrony between channels of high-frequency firing. In both the lamellar and septotemporal directions, Channels 1 and 2 and Channels 3 and 4 were more synchronized than other pairings (Fig. 5*D*,*E*) because Channels 1 and 2 and Channels 3 and 4 were closer to each other, whereas Channels 2 and 3 contained an extra layer of superglue between them. Therefore, the synchronization was the highest between Channels 1 and 2, and Channels 3 and 4.

In the lamellar configuration (Fig. 5*D*), the statistical analysis between groups indicated that the strength of ES in pairs 1 and 3, 1 and 4, and 2 and 3 during the early stages of kindling was significantly different from ES of these pairs during fully kindled stage ($p < 0.05$, ANOVA). There was no significant difference in synchrony strength between the different stages of kindling in the septotemporal configuration (Fig. 5*E*).

Synchrony decreases after phenytoin injection

We then measured the effects of two antiseizure drugs, phenytoin ($n = 4$ rats) and levetiracetam (LEV, $n = 4$ rats), on synchrony along the lamellar axis during kindled seizures. Animals were fully kindled before drug treatment testing. After drug injection,

←

septotemporal configuration were evenly distributed between 0 and 2 pi for early and fully kindled stages. A preferred firing phase was not seen in either stage. ***I***, Theta phase difference distributions were Gaussian distributed ~0, which means that there was no propagation pattern in the septotemporal direction.

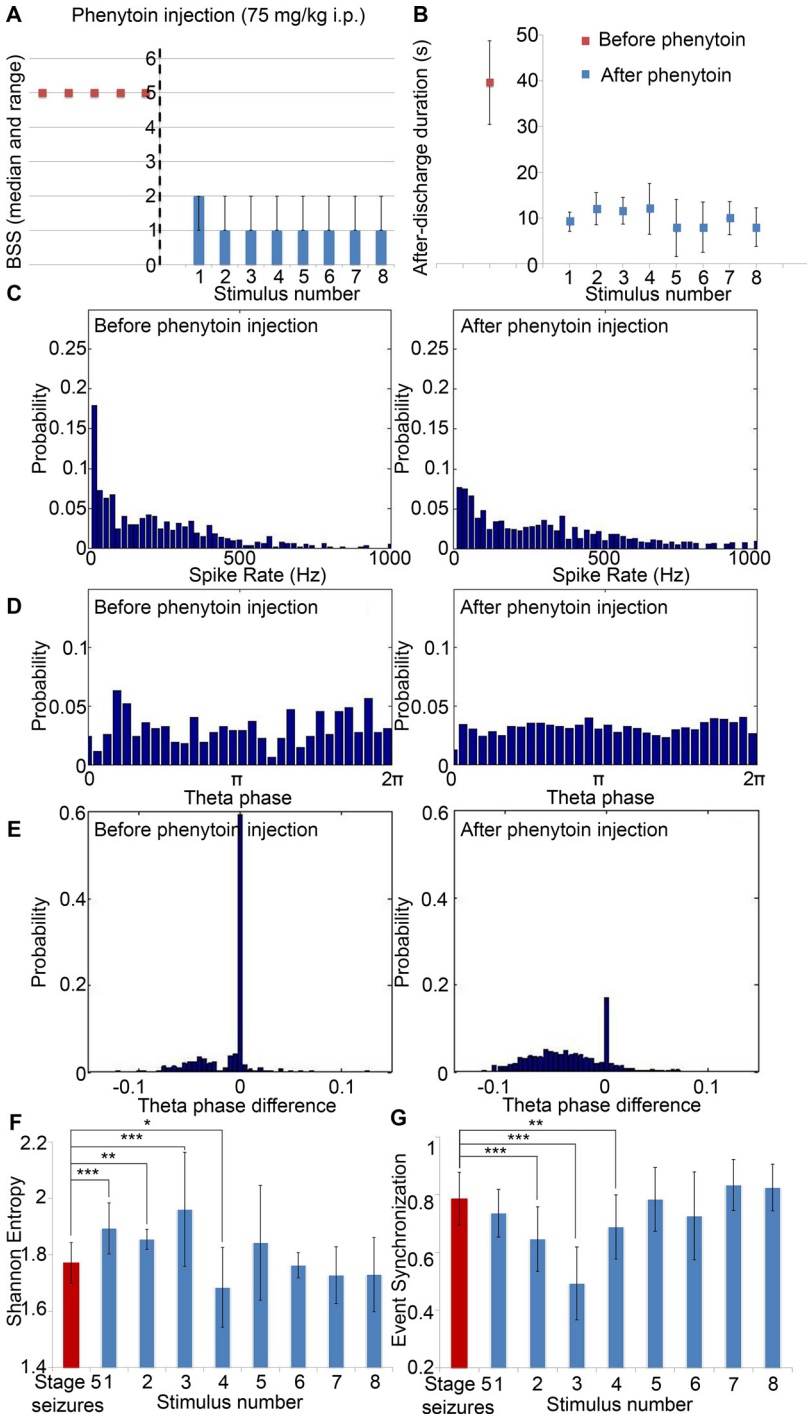

Figure 6. Synchrony decreases after phenytoin injection. ***A***, After the phenytoin treatment, BSS dropped from Stage 5 to Stage 1 or Stage 2. ***B***, After the phenytoin treatment, ADD was reduced to a lower value. ***C***, Spike rate before and after the phenytoin treatment. ***D***, Theta phase distribution before and after phenytoin injection. The preferred firing phase was lost after the phenytoin treatment. ***E***, Theta phase difference distribution before and after phenytoin treatment. Both distributions were negatively skewed. Also, the population ~0 was reduced in the distribution after the phenytoin injection. ***F***, Shannon entropy increased after the treatment for the first 1.5 h and returned to the pre-injection level after 2 h. Red bar represents the Shannon entropy of the Stage 5 seizures. Blue bar represents the entropy of the evoked seizures after the phenytoin treatment. ***G***, ES before and after phenytoin injection. The synchrony decreased after treatment for the first 2 h, then returned to the pre-injection level. Red bar represents the ES strength of the Stage 5 seizures. Blue bar represents the synchronization levels of successive, post-phenytoin treatment-evoked seizures. $*p < 0.05$. $**p < 0.01$. $***p < 0.001$.

the same stimulus was delivered 8 more times, once every 30 min for 4 h.

Thirty minutes after the phenytoin injection, the BSSs dropped from Stage 5 to Stage 1 or Stage 2 (Fig. 6*A*) and stayed there for 4 h (until the end of the recording). The after-discharge also showed a similar decrease (Fig. 6*B*). The mean ADD was 39.6 ± 9 s for fully kindled seizures. Thirty minutes after phenytoin treatment, the ADD declined to 7.8 ± 3.2 s. This seizure duration was maintained over the remaining 4 h of the recording. The spike rate of the seizures after the treatment dropped (Fig. 6*C*, $p < 0.05$, Kolmogorov–Smirnov test). The low-frequency component (<10 Hz) was reduced, and the high-frequency component (>300 Hz) increased.

Theta phase analysis robustly demonstrated that neuronal synchrony decreased after phenytoin treatment. The preferred firing phase value, which occurred around the trough of theta oscillation, was lost after the phenytoin treatment (Fig. 6*D*), and the theta phase distribution became evenly spread between 0 and 2 as well. However, the preferred firing phase returned 2 h later as synchrony returned to the pre-injection levels.

Theta phase differences were calculated between all possible channel pairings (a total of 6). First, all of these distributions were negatively skewed before and after the phenytoin treatment (Fig. 6*E*). The median and mean were negative for all distributions, which indicates that the firing recorded by one channel leads to the other channel. The firings propagated through the transverse extent of the monitored CA1 cell layer, from proximal to distal, which suggests that phenytoin does not affect this propagation pattern. Second, theta phase distribution showed a reduced population ~0 after the phenytoin injection, likely because there was a longer time delay between recording sites because of the decrease in neuronal synchronization.

Order, and therefore synchrony, was quantified by calculating the Shannon entropy of the theta phase distributions. The Shannon entropy of the evoked seizures was significantly different from that of the Stage 5 seizures before the injection was made ($p < 0.05$, ANOVA), for the first 2 h after phenytoin treatment (Fig. 6*F*). The mean Shannon entropy increased for the first 1.5 h. After 2 h, the Shannon entropy recovered to the pre-injection level.

Thirty minutes after phenytoin treatment, the ES strength was similar to that of the Stage 5 seizures before the injection (Fig. 6*G*, $p = 0.097$, ANOVA). However, by 1-2 h after injection, the mean synchrony was attenuated and reached its lowest value at ~1.5 h after injection ($p < 0.01$, ANOVA). Synchrony values slowly began to return to pre-

injection levels 2 h after injection. We also observed this trend in the theta phase analysis. Even when seizure behavior (BSS) and duration (ADD) were suppressed by phenytoin, the synchronization between the firings started to come back.

Synchrony decreases after LEV injection

As with the phenytoin-treated animals, the animals that received an injection of LEV ($n = 4$ rats) displayed a marked and rapid decrease in behavioral seizure stage, falling from Stage 5 at the time of injection to 2 (30 min later) (Fig. 7*A*). The seizure severity of LEV-treated animals began to increase ~1 h after injection. By the end of the recording, 3 of 4 rats had recovered to Stage 5 behavioral seizures. The ADD also decreased significantly after the LEV treatment (Fig. 7*B*). The mean ADD was 91.6 ± 20.3 s for Stage 5 seizures. Thirty minutes after LEV injection, the mean ADD reduced to 50.1 ± 13.7 s. However, unlike BSS, ADD remained at reduced levels, averaging 45.3 ± 17.2 s at the end of the recording, 4 h later.

LEV also altered the spike frequency composition of evoked seizures similarly to phenytoin ($p < 0.05$, Kolmogorov–Smirnov test) (Fig. 7*C*). The low-frequency component (<10 Hz) was reduced, while the high-frequency component (>300 Hz) increased.

The preferred firing phase value, which occurs around the trough of the theta oscillations, was lost after LEV treatment (Fig. 7*D*). The theta phase distribution became evenly spread between 0 and 2 after the injection. The preferred firing phase returned 3 h after the injection, so the theta phase synchronization and BSS returned to pretreatment level around the same time, while ADD remained suppressed by LEV.

Theta phase differences were calculated between all possible channel pairings. There was no significant difference before and after the LEV treatment (Fig. 7*E*). The distributions were negatively skewed before and after LEV injection, indicating that the propagation pattern was not affected by the administration of LEV. There was also no difference between the mean, median, or skewness of the distribution ($p < 0.05$, ANOVA). This observation contrasts with the phenytoin-treated animals that showed differences in phase difference distributions before and after the treatment.

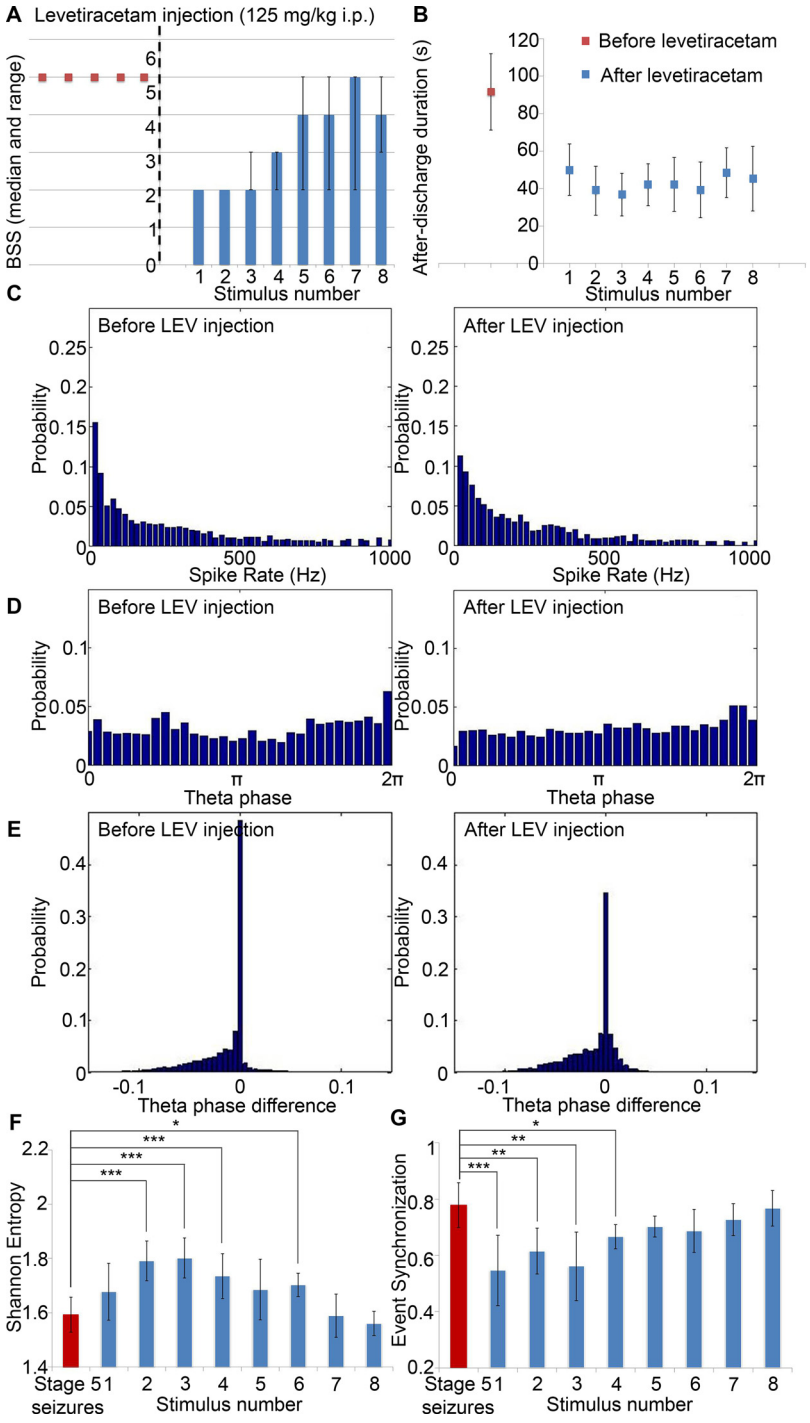

Figure 7. Synchrony decreases after LEV injection. ***A***, After the LEV treatment, BSS dropped from Stage 5 to Stage 2 before recovering back to Stages 4 and 5. ***B***, After the LEV treatment, ADD fell to lower values. ***C***, Spike rate before and after the LEV treatment. ***D***, Theta phase distribution before and after LEV injection. The preferred firing phase was initially lost after the LEV treatment, although it returned 3 h after injection. ***E***, Theta phase difference distribution before and after the LEV treatment. ***F***, Shannon entropy increased after the treatment for the first 1.5 h before returning to the pre-injection levels. Red bar represents the Shannon entropy of the Stage 5 seizures. Blue bar represents the entropy of the evoked seizures after the LEV treatment. ***G***, ES before and after the LEV treatment. The synchrony decreased after the treatment for the first 2 h and then returned to pre-injection levels. Red bar represents the ES strength of the Stage 5 seizures. Blue bar represents the ES after the LEV treatment. $^{*}p < 0.05$. $^{**}p < 0.01$. $^{***}p < 0.001$.

The Shannon entropy of the evoked seizures was significantly different from that of the Stage 5 seizures before the injection ($p < 0.001$, ANOVA), for the first 2 h after LEV, as shown in Figure 7*F*. The mean Shannon entropy increased for the first 1.5 h after the treatment, which indicates that the evoked seizures become less synchronized than the Stage 5 seizures. However, this was temporary, as the mean Shannon entropy started to decrease and returned to the pre-injection level after 3 h.

ES fell to a lower value over 2 h immediately following the LEV treatment and then slowly returned to its pre-injection value (Fig. 7*G*). The initial decrease in the strength of ES was significant ($p < 0.05$, ANOVA) compared with the behavioral Stage 5 seizures before the injection. It remained so for the duration of the first 2 h after treatment, after which it returned to its pre-injection levels. This return to baseline was also apparent in the theta phase analysis.

Discussion

We found that, in the lamellar direction, neuronal firing is maximally correlated during the middle phase of a seizure, while both the beginning and the end of a seizure were less correlated, indicating that synchrony evolves dynamically during seizures. We found that neurons were more correlated along the lamellar axis than those along the septotemporal axis, suggesting that neurons' firings are not synchronized homogeneously across locations.

Neuronal activity during a seizure is complex, high-dimensional, nonlinear, nonstationary, and noisy (Osorio and Lai, 2011). It was hypothesized that seizures result from the hypersynchronous firing of neurons (Penfield and Jasper, 1954). However, several studies have suggested that seizures may involve both synchronized and desynchronized neuronal dynamics (Le Van Quyen et al., 2001; Netoff and Schiff, 2002; Schiff et al., 2005; Frei et al., 2010; Cymerblit-Sabba and Schiller, 2012). More recently, network theories were applied to understand seizure dynamics using the concept of epileptic network synchronizability (Khambhati et al., 2016; Kini et al., 2019). These studies identify brain regions that push-pull synchronizing or a desynchronizing role in shaping seizure spread. The current study suggests CA1 pyramidal neurons connected along lamella may act as synchronizing nodes.

The lamellar hypothesis argues that hippocampal cells are activated in a stripe-like fashion and that the principal excitatory pathways of the hippocampus are organized in a lamellar fashion (Andersen et al., 1971). With the development of intact *in vitro* hippocampal preparation, the intrahippocampal epileptiform activity propagated in both the lamellar and septotemporal directions (Andersen et al., 2000; Derchansky et al., 2006; Kibler and Durand, 2011). However, the lamellar hypothesis had not previously been tested in whole animals. To further study seizure propagation in the hippocampal CA1 cell layer, we investigated neuronal synchrony in both lamellar and septotemporal directions in awake rats. The complex structure underlying seizure propagation was explored by theta phase synchronization. We discovered that neuronal firing in the hippocampal CA1 propagates along the lamellar axis, from proximal to distal in the hippocampus CA1 region. Proximal CA1 is the part of CA1 that is close to CA3. This pattern indicates that seizures originate in the hippocampal CA3 because of direct CA3 stimulation and then propagate through the transverse extent of the monitored CA1 cell layer. However, no propagation pattern was observed along the septotemporal axis.

These findings suggest that evoked seizures primarily propagate along the lamellar axis. Sloviter and Lømo (2012) argue that septotemporal connections are inhibitory, while lamellar connections are excitatory. Thus, our findings support the connectivity hypothesis that excitatory anatomic connections of the seizure focus drive seizure spread. This hypothesis is not only limited to the hippocampal circuit as our previous work in frontal lobe spontaneous seizures also supports it (Brodovskaya et al., 2021). Interestingly, we revealed that the propagation pattern is preserved in the lamellar direction throughout the kindling process, while no rapid propagation pattern is observed or emerges in the septotemporal direction. Therefore, for the first time, a two-dimensional propagation structure of neuronal firing was discovered during kindling. We conclude that the lamellar organization remains a useful concept for understanding the propagation of hippocampal neuronal firings during kindling, and the synchrony structure during seizures and epileptogenesis depends on anatomic connectivity and plasticity.

This connectivity hypothesis is further supported by earlier observations that mossy fiber sprouting extends septotemporally for 600-700 μm in chronic models of kainic acid and kindling, connecting lamella which normally have little or no connectivity (Sutula et al., 1998). The formation of excitatory "detonator" sprouted mossy fiber synapses has recently been demonstrated to potentially contribute to recurrent excitation across septotemporal lamella (Hendricks et al., 2019).

Generally, synchronization measurements are either linear or nonlinear. Linear correlation evaluates linear relationships, whereas nonlinear synchronization reveals a nonlinear functional relationship between the dynamics of two systems (Rulkov et al., 1995). Schiff et al. (1996) explained that nonlinear synchronization is a better candidate for complex neuronal systems, such as seizures, but whether the linear or nonlinear method is better at detecting synchronization in epilepsy remains an open area.

We were interested in three different methods for synchrony measurement: cross-correlation, ES, and phase synchronization. Cross-correlation is the most commonly used linear measurement of synchrony that studies the similarity of two waveforms, calculating the correlation between local field potentials (Adhikari et al., 2010). Time delays and phase synchronization are two commonly used nonlinear methods. ES is based on time delays to determine seizure severity and network dynamics (Quian Quiroga et al., 2002). We selected a novel synchrony measurement for phase synchronization, theta phase synchronization, as an underlying clock in the hippocampus. Theta oscillations are essential for the hippocampus's normal functioning and function as a clock for hippocampal activity during exploration (O'Keefe and Dostrovsky, 1971; O'Keefe and Conway, 1978; O'Keefe and Recce, 1993). The theta rhythm, a hippocampal network pattern in the 4-10 Hz frequency band, is often recognized as the defining electrophysiological signature of hippocampal activity during temporal coding/decoding of active neuron ensembles. The extracellular currents underlying theta waves are generated mainly by the entorhinal input, CA3 Schaffer collateral, and voltage-dependent Ca^{2+} currents in pyramidal cell dendrites (Bazsaki, 2002). We then used Shannon entropy to calculate the order of the phase distribution, which was then used to describe the synchrony of the system.

Theta phase synchronization revealed that, in the lamellar direction, the hippocampal CA1 neurons tend to fire around the theta oscillations' negative peaks at the end of kindling while having no preference at the beginning of kindling. However, in the septotemporal direction, the neuronal firings did not interact with the underlying theta oscillations, and no preferred firing phase was observed during kindling. The development of a preferred firing phase along the lamellar axis indicates that local neuronal firings became strongly influenced by the slow theta oscillations. Additionally, the marked transition from unaffected to strongly affected indicates that the firings became more organized along the lamellar axis as kindling progressed.

Phenytoin obstructs recurrent action potentials by blocking voltage-dependent sodium channels (Yaari et al., 1986; Macdonald and Kelly, 1993). LEV has multiple mechanisms of action, but it binds the synaptic vesicle protein 2, the loss of which decreases the synaptic strength specifically during high-frequency firing (Madeja et al., 2003; Lynch et al., 2004; Custer et al., 2006; C. Y. Lee et al., 2009). Since LEV inhibits synaptic excitation, LEV has been shown to depress field potentials *in vitro*, suggesting that it might act against interneuronal synchronization (Niespodziany et al., 2003).

We found that phenytoin and LEV decreased synchrony *in vivo*, and the preferred firing phase value (around the trough of the theta oscillation) was lost within the first 2-3 h of drug treatment before recovering to pretreatment levels. However, the firing propagation pattern remained the same from proximal to distal CA1 cell layer after both treatments, suggesting that both treatments do not affect the propagation pattern. Synchrony returned to pretreatment levels before behavioral or electrographic seizures, suggesting that greater synchrony drives more severe seizures consistent with the push-pull hypothesis (Khambhati et al., 2016).

Approximately one-third of epilepsy patients do not respond favorably to currently available drug treatments, and up to 50% experience side effects of these antiepileptic drugs (Y. Li and Mogul, 2007). Currently, deep brain stimulation therapy is an alternative method to terminate seizures by desynchronizing groups of neurons (Gluckman et al., 2001; Theodore and Fisher, 2004; Colpan et al., 2007; Fisher et al., 2010), but there is uncertainty on which groups of neurons fire synchronously or chaotically during seizures, so the efficacy of brain stimulation can be improved. For example, electrical stimulation is more likely to terminate a seizure when stimulation is applied close to the negative peak (Motamedi et al., 2002). Here, we show that neurons linked by excitatory connections fire synchronously during seizures, and the synchrony structure during seizures depends on anatomic connectivity and plasticity. Thus, closed-loop brain stimulation precisely targeted to disrupt synchrony may improve treatment outcomes.

References

Adhikari A, Sigurdsson T, Topiwala MA, Gordon JA (2010) Cross-correlation of instantaneous amplitudes of field potential oscillations: a straightforward method to estimate the directionality and lag between brain areas. J Neurosci Methods 191:191–200.

Andersen P, Bliss TV, Skrede KK (1971) Lamellar organization of hippocampal excitatory pathways. Exp Brain Res 13:222–238.

Andersen P, Soleng AF, Raastad M (2000) The hippocampal lamella hypothesis revisited. Brain Res 886:165–171.

Andersen P, Morris R, Amaral D, Bliss T, O'Keefe J (2009) The hippocampus book. Oxford: Oxford UP.

Bazsaki G (2002) Theta oscillations in the hippocampus. Neuron 33:325–340.

Brette R, Destexhe A (2012) Handbook of neural activity measurement. Cambridge: Cambridge UP.

Brodovskaya A, Shiono S, Kapur J (2021) Activation of the basal ganglia and indirect pathway neurons during frontal lobe seizures. Brain awab119.

Colpan ME, Li Y, Dwyer J, Mogul DJ (2007) Proportional feedback stimulation for seizure control in rats. Epilepsia 48:1594–1603.

Custer KL, Austin NS, Sullivan JM, Bajjalieh SM (2006) Synaptic vesicle protein 2 enhances release probability at quiescent synapses. J Neurosci 26:1303–1313.

Cymerblit-Sabba A, Schiller Y (2012) Development of hypersynchrony in the cortical network during chemoconvulsant-induced epileptic seizures in vivo. J Neurophysiol 107:1718–1730.

De Curtis M, Avanzini G (2001) Interictal spikes in focal epileptogenesis. Prog Neurobiol 63:541–567.

Derchansky M, Rokni D, Rick JT, Wennberg R, Bardakjian BL, Zhang L, Yarom Y, Carlen PL (2006) Bidirectional multisite seizure propagation in the intact isolated hippocampus: the multifocality of the seizure 'focus.' Neurobiol Dis 23:312–328.

Fisher R, Salanova V, Witt T, Worth R, Henry T, Gross R, Oommen K, Osorio I, Nazzaro J, Labar D, Kaplitt M, Sperling M, Sandok E, Neal J, Handforth A, Stern J, DeSalles A, Chung S, Shetter A, Bergen D, et al. (2010) Electrical stimulation of the anterior nucleus of thalamus for treatment of refractory epilepsy. Epilepsia 51:899–908.

Fisher R, Scharfman HE, Decurtis M (2014) How can we identify ictal and interictal abnormal activity? Adv Exp Med Biol 813:3–23.

Frei MG, Zaveri HP, Arthurs S, Bergey GK, Jouny CC, Lehnertz K, Gotman J, Osorio I, Netoff TI, Freeman WJ, Jefferys J, Worrell G, Van Quyen ML, Schiff SJ, Mormann F (2010) Controversies in epilepsy: debates held during the Fourth International Workshop on Seizure Prediction. Epilepsy Behav 19:4–16.

Gluckman BJ, Nguyen H, Weinstein SL, Schiff SJ (2001) Adaptive electric field control of epileptic seizures. J Neurosci 21:590–600.

Hendricks WD, Westbrook GL, Schnell E (2019) Early detonation by sprouted mossy fibers enables aberrant dentate network activity. Proc Natl Acad Sci USA 116:10994–10999.

Herberg LJ, Rose IC (1994) Kindled epileptic seizures, postictal refractoriness, status epilepticus, and electrical self-stimulation. Neurosci Biobehav Rev 18:411–420.

Johnson SE, Hudson JL, Kapur J (2015) Synchronization of action potentials during low-magnesium-induced bursting. J Neurophysiol 113:2461–2470.

Johnston D, Brown TH (1984) The synaptic nature of the paroxysmal depolarizing shift in hippocampal neurons. Ann Neurol 16:S65–S71.

Khambhati AN, Davis KA, Lucas TH, Litt B, Bassett DS (2016) Virtual cortical resection reveals push-pull network control preceding seizure evolution HHS Public Access. Neuron 91:1170–1182.

Kibler AB, Durand DM (2011) Orthogonal wave propagation of epileptiform activity in the planar mouse hippocampus in vitro. Epilepsia 52:1590–1600.

Kini LG, Bernabei JM, Mikhail F, Hadar P, Shah P, Khambhati AN, Oechsel K, Archer R, Boccanfuso J, Conrad E, Shinohara RT, Stein JM, Das S, Kheder A, Lucas TH, Davis KA, Bassett DS, Litt B (2019) Virtual resection predicts surgical outcome for drug-resistant epilepsy. Brain 142:3892–3905.

Lee CY, Chen CC, Liou HH (2009) Levetiracetam inhibits glutamate transmission through presynaptic P/Q-type calcium channels on the granule cells of the dentate gyrus. Br J Pharmacol 158:1753–1762.

Lee D (2002) Analysis of phase-locked oscillations in multi-channel single-unit spike activity with wavelet cross-spectrum. J Neurosci Methods 115:67–75.

Lenck-Santini PP, Holmes GL (2008) Altered phase precession and compression of temporal sequences by place cells in epileptic rats. J Neurosci 28:5053–5062.

Le Van Quyen M, Martinerie J, Navarro V, Baulac M, Varela FJ (2001) Characterizing neurodynamic changes before seizures. J Clin Neurophysiol 18:191–208.

Li X, Cui D, Jiruska P, Fox JE, Yao X, Jefferys JG (2007) Synchronization measurement of multiple neuronal populations. J Neurophysiol 98:3341–3348.

Li Y, Mogul DJ (2007) Electrical control of epileptic seizures. J Clin Neurophysiol 24:197–204.

Lothman EW, Hatlelid JM, Zorumski CF, Conry JA, Moon PF, Perlin JB (1985) Kindling with rapidly recurring hippocampal seizures. Brain Res 360:83–91.

Lynch BA, Lambeng N, Nocka K, Kensel-Hammes P, Bajjalieh SM, Matagne A, Fuks B (2004) The synaptic vesicle is the protein SV2A is the binding site for the antiepileptic drug levetiracetam. Proc Natl Acad Sci USA 101:9861–9866.

Macdonald RL, Kelly KM (1993) Antiepileptic drug mechanisms of action. Epilepsia 34:S1–S8.

Madeja M, Margineanu DG, Gorji A, Siep E, Boerrigter P, Klitgaard H, Speckmann EJ (2003) Reduction of voltage-operated potassium currents by levetiracetam: a novel antiepileptic mechanism of action? Neuropharmacology 45:661–671.

McCormick DA, Contreras D (2001) On the cellular and network bases of epileptic seizures. Annu Rev Physiol 63:815–846.

Merricks EM, Smith EH, McKhann GM, Goodman RR, Bateman LM, Emerson RG, Schevon CA, Trevelyan AJ (2015) Single unit action potentials in humans and the effect of seizure activity. Brain 138:2891–2906.

Miles R, Wong RK, Traub RD (1984) Synchronized afterdischarges in the hippocampus: contribution of local synaptic interactions. Neuroscience 12:1179–1189.

Motamedi GK, Lesser RP, Miglioretti L, Mizuno-Matsumoto Y, Gordon B, Webber WR, Jackson DC, Sepkuty JP, Crone NE (2002) Optimizing parameters for terminating cortical afterdischarges with pulse stimulation. Epilepsia 43:836–846.

Netoff TI, Schiff SJ (2002) Decreased neuronal synchronization during experimental seizures. J Neurosci 22:7297–7307.

Niespodziany I, Klitgaard H, Margineanu DG (2003) Desynchronizing effect of levetiracetam on epileptiform responses in rat hippocampal slices. Neuroreport 14:1273–1276.

O'Keefe J, Conway DH (1978) Hippocampal place units in the freely moving rat: why they fire where they fire. Exp Brain Res 31:573–590.

O'Keefe J, Dostrovsky J (1971) The hippocampus as a spatial map: preliminary evidence from unit activity in the freely-moving rat. Brain Res 34:171–175.

O'Keefe J, Recce ML (1993) Phase relationship between hippocampal place units and the EEG theta rhythm. Hippocampus 3:317–330.

Osorio I, Lai YC (2011) A phase-synchronization and random-matrix based approach to multichannel time-series analysis with application to epilepsy. Chaos 21:033108.

Penfield W, Jasper HH (1954) Epilepsy and the functional anatomy of the human brain. Boston: Little, Brown.

Pottkämper JC, Hofmeijer J, van Waarde JA, van Putten MJ (2020) The postictal state: what do we know? Epilepsia 61:1045–1061.

Quian Quiroga R, Kreuz T, Grassberger P (2002) Event synchronization: a simple and fast method to measure synchronicity and time delay patterns. Phys Rev E Stat Nonlin Soft Matter Phys 66:041904.

Racine RJ (1972) Modification of seizure activity by electrical stimulation: II. Motor seizure. Electroencephalogr Clin Neurophysiol 32:281–294.

Richardson TL, Turner RW, Miller JJ (1987) Action-potential discharge in hippocampal CA1 pyramidal neurons: current source-density analysis. J Neurophysiol 58:981–996.

Rulkov NF, Sushchik MM, Tsimring LS, Abarbanel HD (1995) Generalized synchronization of chaos in directionally coupled chaotic systems. Phys Rev E Stat Phys Plasmas Fluids Relat Interdiscip Topics 51:980–994.

Schevon CA, Trevelyan AJ (2014) The cellular basis of EEG. In: Current practice of clinical electroencephalography, Ed 4, pp 1–27. Philadelphia: Wolters Kluwer Health.

Schevon CA, Weiss SA, McKhann G, Goodman RR, Yuste R, Emerson RG, Trevelyan AJ (2012) Evidence of an inhibitory restraint of seizure activity in humans. Nat Commun 3:1060.

Schiff SJ, Sauer T, Kumar R, Weinstein SL (2005) Neuronal spatiotemporal pattern discrimination: the dynamical evolution of seizures. Neuroimage 28:1043–1055.

Schiff SJ, So P, Chang T, Burke RE, Sauer T (1996) Detecting dynamical interdependence and generalized synchrony through mutual prediction in a neural ensemble. Phys Rev E Stat Phys Plasmas Fluids Relat Interdiscip Topics 54:6708–6724.

Sloviter RS, Lømo T (2012) Updating the lamellar hypothesis of hippocampal organization. Front Neural Circuits 6:1–16.

Sloviter RS, Zappone CA, Harvey BD, Frotscher M, Sloviter RS (2006) Kainic acid-induced recurrent mossy fiber innervation of dentate gyrus GABAergic interneurons: a possible anatomical substrate of granule cell hyperinhibition in chronically epileptic rats. J Comp Neurol 494:944–960.

Sutula T, Zhang P, Lynch M, Sayin U, Golarai G, Rod R (1998) Synaptic and axonal remodeling of mossy fibers in the hilus and supragranular region of the dentate gyrus in kainate-treated rats. J Comp Neurol 390:578–594.

Theodore WH, Fisher RS (2004) Brain stimulation for epilepsy. Lancet Neurol 3:111–118.

Traub RD, Wong RK (1982) Cellular mechanism of neuronal synchronization in epilepsy. Science 216:745–747.

Traub RD, Miles R, Wong RK (1989) Model of the origin of rhythmic population oscillations in the hippocampal slice. Science 243:1319–1325.

Truccolo W, Donoghue JA, Hochberg LR, Eskandar EN, Madsen JR, Anderson WS, Brown EN, Halgren E, Cash SS (2011) Single-neuron dynamics in human focal epilepsy. Nat Neurosci 14:635–643.

Wong RK, Traub RD, Miles R (1986) Cellular basis of neuronal synchrony in epilepsy. Adv Neurol 44:583–592.

Yaari Y, Selzer ME, Pincus JH (1986) Phenytoin: mechanisms of its anticonvulsant action. Ann Neurol 20:171–184.